

# Adaptive technique for change detection in VHR multispectral images robust to registration noise

Francesca Bovolo, Silvia Marchesi and Lorenzo Bruzzone

**Abstract**— This paper presents an automatic context-sensitive technique robust to registration noise ( $RN$ ) for change detection (CD) in multitemporal very high geometrical resolution (VHR) remote-sensing images. Exploiting the properties of  $RN$  in VHR images, the proposed technique analyzes the distribution of the spectral change vectors (SCVs) computed according to the change vector analysis in an adaptively quantized polar domain. The method studies the behavior of SCVs falling into each quantization cell at different resolution levels (scales) in the polar domain to automatically reduce the effects of  $RN$  on the final change detection map. This information is jointly exploited with the spatial-context information contained in the neighborhood of each pixel for generating the final CD map. The spatial-context information is modeled through the definition of adaptive regions homogeneous both in spatial and temporal domain (parcels). Experimental results obtained on real VHR remote-sensing multitemporal images confirm the effectiveness of the proposed approach.

**Index Terms**— Multitemporal images, very high resolution images, change detection, change vector analysis, registration noise, remote sensing.

## I. INTRODUCTION

UNSUPERVISED change detection plays an important role in many application domains related to the exploitation of multitemporal images (e.g., in video surveillance [1],[2], motion detection [3], remote sensing [4],[5], biomedical applications [6], etc). For some domains, as the remote sensing and the biomedical ones, the change-detection procedure should deal with multichannel images. Identifying changes in multidimensional vectors associated with each pixel of the investigated multitemporal images becomes a complex task.

In this paper we focus the attention on unsupervised change-detection technique for multitemporal and multispectral VHR remote sensing image acquired by the last generation satellites (e.g., Ikonos, Quickbird, EROS, SPOT-5, GeoEye-1, WorldView). Resolution on the ground varies from few meters to 41[cm] in the best case. This behavior make the most the unsupervised change-detection methods for multidimensional remote-sensing images presented in the literature [7]-[10] ineffective. This is because they were optimized for medium geometrical resolution images and therefore assume spatial independence among pixels and do not model the multiscale nature of the scene. However in VHR images spatial correlation among neighboring pixels and multiscale properties of the scene should be considered to get accurate and reliable CD maps [14]-[16].

When dealing with CD in multispectral optical images, other critical issues to be faced arise from differences in sunlight and atmospheric conditions as well as in sensor

acquisition geometry [5],[11]. In order to reduce their impact on CD maps, pre-processing steps are required as: co-registration, radiometric and geometric corrections, and noise reduction. Among them, co-registration plays a fundamental role and becomes more complex and critical (and therefore intrinsically less accurate), when dealing with VHR images. In practice, a perfect alignment between images is impossible as differences in the acquisition view angles and in geometrical distortions cannot be compensated causing a significant residual  $RN$  which sharply impacts on CD [11],[12],[13].

In order to overcome the aforementioned problems, this paper presents an adaptive context-sensitive technique, which: i) reduces the impact of  $RN$  on change detection in VHR multispectral images through a multiscale strategy; ii) considers the spatial dependencies of neighboring pixels through the definition of multitemporal parcels (i.e., region homogeneous both in space and time). The proposed technique is developed in the context of the polar framework for change vector analysis (CVA) introduced in [17] and is based on the analysis of the properties of  $RN$  presented in [18]. The experiments carried out on multitemporal VHR images confirm the validity of the theoretical analysis and the effectiveness of the proposed technique.

The paper is organized into five sections. The next one recalls: notation and background of the polar framework [17]; and the registration noise properties [18]. Section III illustrates the proposed multiscale and context-based approach for change detection on VHR images. Section IV presents the validation on real multitemporal Quickbird images of both the multiscale properties of  $RN$  and the proposed CD technique. Finally, section V draws the conclusions of this work.

## II. NOTATION AND BACKGROUND

In order to develop the proposed CD technique robust to registration noise, we take advantage of the theoretical polar framework for CVA in the polar domain proposed in [17] and of the theoretical and empirical analysis on the properties of this kind of noise conducted in [18]. In the following we briefly recall the main concepts of this framework and the main properties of registration noise. For simplicity, the whole analysis is carried out considering a 2-dimensional feature space (however it can be generalized to the case of more dimensions, see [17]).

### A. Polar framework for change detection

Let us consider two VHR multispectral images  $\mathbf{X}_1$  and  $\mathbf{X}_2$  acquired over the same geographical area at different times  $t_1$  and  $t_2$ , respectively. Assume that these images do not show significant radiometric differences. Let  $\Omega = \{\omega_n, \Omega_c\}$  be the set

of classes of changed and unchanged pixels to be identified.  $\omega_n$  represents the class of unchanged pixels and  $\Omega_c = \{\omega_{c_1}, \dots, \omega_{c_k}\}$  the set of the  $K$  possible classes (kinds) of changes occurred in the considered area. Let  $\mathbf{X}_D$  be the multispectral difference image computed according to the CVA technique by subtracting the spectral feature vectors associated with each corresponding spatial position in  $\mathbf{X}_1$  and  $\mathbf{X}_2$ .  $\mathbf{X}_D$  is a multidimensional image made up of spectral change vectors (SCVs) defined as:

$$\mathbf{X}_D = \mathbf{X}_2 - \mathbf{X}_1 \quad (1)$$

In a 2-dimensional feature space, the change information contained in a generic SCVs  $s$  can be univocally described by the change vector magnitude  $\rho$  and direction  $\vartheta$  defined as:

$$\vartheta = \tan^{-1} \left( \frac{\mathbf{X}_{1,D}}{\mathbf{X}_{2,D}} \right) \quad \text{and} \quad \rho = \sqrt{(\mathbf{X}_{1,D})^2 + (\mathbf{X}_{2,D})^2} \quad (2)$$

where  $\mathbf{X}_{b,D}$  is the  $b$ th component (spectral channel) of  $\mathbf{X}_D$  ( $b = \{1, 2\}$ ). Finally, let us define the magnitude-direction domain  $MD$  (in which all the SCVs of a given scene are included) as:

$$MD = \{\rho \in [0, \rho_{\max}] \text{ and } \vartheta \in [0, 2\pi]\} \quad (3)$$

where  $\rho_{\max}$  is the highest magnitude of SCVs in the considered images.

According to [17] and under the above-mentioned assumptions, unchanged and changed SCVs result in separated clusters in the polar representation. Unchanged SCVs show a low magnitude, are uniformly distributed with respect to  $\vartheta$  and fall in the *circle of no-changed pixels*  $C_n$ :

$$C_n = \{\rho, \vartheta : 0 < \rho \leq T \text{ and } 0 \leq \vartheta < 2\pi\} \quad (4)$$

This circle is centered at the origin and has a radius equal to the optimal (in the sense of the theoretical Bayesian decision theory) threshold  $T$  that separates unchanged from changed pixels. On the opposite, changed SCVs are expected to show a high magnitude and fall in the *annulus of changed pixels*  $A_c$ :

$$A_c = \{\rho, \vartheta : T \leq \rho < \rho_{\max} \text{ and } 0 \leq \vartheta < 2\pi\} \quad (5)$$

This annulus has inner radius  $T$  and outer radius given by  $\rho_{\max}$ . As unchanged SCVs show preferred directions according to the kind of change, different kinds of changes can be isolated with a pair of threshold values ( $\vartheta_{k_1}$  and  $\vartheta_{k_2}$ ) in the direction domain. Each pair of thresholds identifies, in  $A_c$ , an *annular sector*  $S_k$  of change  $\omega_k \in \Omega_c$  ( $k=1, \dots, K$ ):

$$S_k = \{\rho, \vartheta : \rho \geq T \text{ and } \vartheta_{k_1} \leq \vartheta \leq \vartheta_{k_2}, 0 \leq \vartheta_{k_1} < \vartheta_{k_2} \leq 2\pi\} \quad (6)$$

All the mentioned regions are depicted in Fig. 1. The reader is referred to [17] for further details.

### B. Registration noise properties

As previously mentioned, residual misregistration affects multitemporal data and represents an important source of noise especially in VHR multitemporal images. *RN* is due to the comparison of corresponding pixels that do not represent the same area on the ground. According to [18] misregistration effects in the polar framework varies with: i) the misalignment between multitemporal images; ii) the resolution (scale) of the images; and iii) and operated differently on changed and

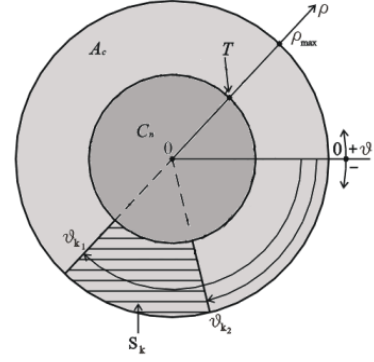


Fig. 1. Representation of the regions of interest in the CVA polar framework

unchanged SCVs.

When the misalignment between the images increase, it is possible to observe that:

1. *RN* affects unchanged pixels by: (a) increasing the spread of the cluster in  $C_n$  with respect to the case of perfectly aligned images; (b) generating clusters of dominant *RN* with properties very similar to clusters of changed pixel in  $A_c$ . The first effect is related to the non-perfect alignment between multitemporal pixels belonging to the same object, while the second one is mainly induced from edge regions and details, which lead to the comparison of pixels belonging to different objects. These pixels generate clusters of *RN* in  $A_c$  and cause false alarms in the CD map. This is the most critical component of *RN*. Therefore it is important to identify such pixels making change detection robust to *RN*.
2. *Statistical properties of clusters associated with changed pixels in  $A_c$  slowly vary with the amount of misalignment.* In other words *RN* does not affect significantly the clusters of changed pixels.

In this work we are more interested on the impact of the scale on registration noise properties. To properly illustrate them let us consider a pansharpened Quickbird image acquired on the city of Trento (Italy) in July 2006 ( $\mathbf{X}_1$ )<sup>1</sup>. From this image a second image was generated ( $\mathbf{X}_2$ ) simulating new houses on the rural area. Such changes were introduced in order to be as similar as possible to real changes. In particular, simulated buildings have been added to the scene taking their geometrical structures and spectral signatures from other real buildings present in the image [18]. Moreover  $\mathbf{X}_1$  and  $\mathbf{X}_2$  were relatively shifted for reproducing registration noise effects in a controlled framework. To both images a *Daubechies-4* stationary wavelet multiscale decomposition [19] was applied in order to obtain a set of multitemporal datasets at different resolution levels (for further details, refer to [18]). The scatterograms in Fig. 2 show the statistical distributions of SCVs obtained according to CVA in the polar domain for the misregistered dataset: (a) at full resolution; and (b) at level 3 of the wavelet decomposition. Comparing the scatterograms it can be observed that reducing the scale, SCVs associated with *RN* (dashed circles in Fig. 2.a) tend to disappear collapsing into  $C_n$ , while the cluster of pixels associated with simulated

<sup>1</sup> For further detail about this image refer to sec. IV.A.

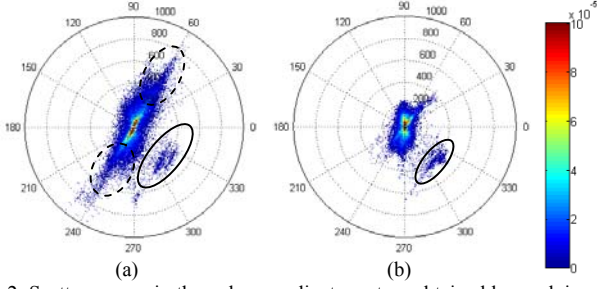


Fig. 2. Scattergrams in the polar coordinate system obtained by applying the CVA technique to the simulated data sets containing changes (a) at full resolution, and (b) at a lower scale.

new buildings (continuous circles in Fig. 2) reduces its spread, but it is not completely smoothed out. This is confirmed from Fig. 3, which shows the behavior of the mean value of the magnitude of SCVs associated with  $RN$  and true changes. As can be seen, by reducing the resolution the mean value of the magnitude of SCVs associated with  $RN$  decreases faster than the one of clusters of changed pixels. Therefore, at low resolution levels (where high spatial frequencies are cut off) the impact of the  $RN$  is lower than at high resolution levels. Accordingly, in  $A_c$  mainly clusters due to spectral changes can be detected. This simple observation suggests us important strategies for the definition of a CD technique robust to  $RN$ .

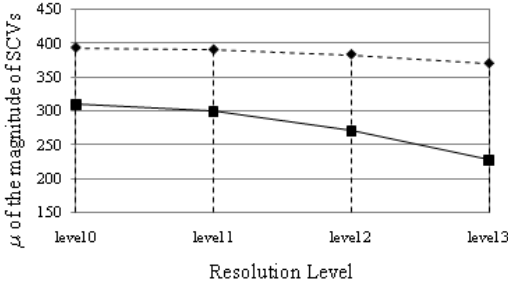


Fig. 3. Behavior of the mean value of the magnitude of SCVs versus the resolution levels (scale) for clusters of change (dashed line) and of registration noise (continuous line).

From the presented analysis and according to [18], two important properties can be derived for what concerns the effects of a scale reduction on the registration noise properties:

3. Clusters associated with registration noise in  $A_c$  exhibit significant variations of properties versus the scale;
4. Clusters of changes exhibit slowly varying statistical properties.

It follows that decreasing the scale the behaviors of changed and unchanged SCVs in  $A_c$  versus the scale are different: sectors of changes, unlike sectors of registration noise, are preserved, i.e., changes show an intrinsic robustness to the scale. This observation holds assuming that, given the very high resolution of images, true significant changes are associated with objects with a non-negligible size, whereas misregistration appears in the difference image with relatively thin structures having different orientations. As the resolution decreases, the impact of the  $RN$  decreases as well.

These last two properties represent the theoretical basis of the approach to change detection robust to registration noise

presented in the next section.

It is worth noting that similar behaviors of registration noise were observed on other data sets (which contain areas with other characteristics and images acquired by other sensors). Therefore these results are omitted for space constraints.

### III. METHODOLOGY

The multiscale properties of  $RN$  briefly recalled in the previous section are at the basis of the development of a change-detection technique robust to  $RN$ . Assuming that true significant changes have a non-negligible size and that misregistration appears in the difference image with relatively thin structures having different orientations reducing the resolution of images, implicitly decreases the presence of  $RN$  with respect to that on the original scene, while true changes maintain a good stability. In other words, the lower is the geometrical resolution, the lower the probability of identifying in  $A_c$  pixels associated with  $RN$ . This means that at low resolution levels in  $A_c$  mainly clusters due to the presence of true changes on the ground can be detected. However, in order to obtain a change-detection map characterized by a good geometrical fidelity, we should work at full resolution.

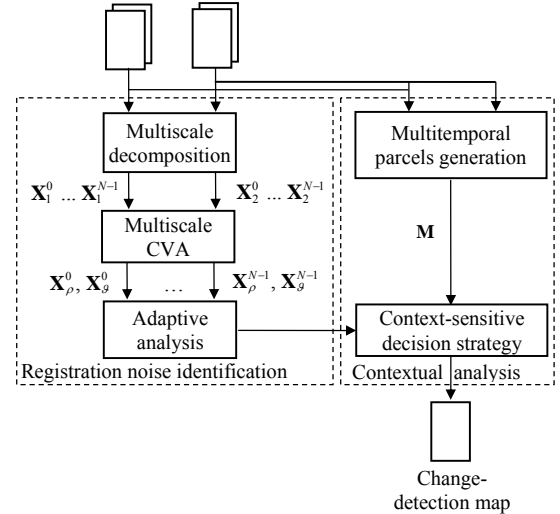


Fig. 4. General architecture of the proposed multiscale and parcel-based change-detection technique.

According to the above observations, we propose an automatic technique for change detection in multitemporal and multispectral VHR images robust to registration noise based on two main phases: i) registration noise identification; and ii) decision strategy for the generation of the final change-detection map. The main idea is to detect the regions of the polar framework where the  $RN$  is dominant according to a multiscale strategy and then to consider the spatial contextual information through the definition of multitemporal parcels at high resolution level in order to generate the final change-detection map with a high detail content (see Fig. 4).

#### A. Registration noise identification

The first phase of the proposed technique aims at identifying

clusters related to  $RN$  in the polar domain. To this purpose, we propose an analysis based on the following four steps: a) quantization of the polar domain into cells of fixed size; b) multiscale decomposition of the VHR multitemporal images; c) analysis of the SCV distributions within each quantization cell at different resolution levels; and d) adaptive estimation of the cell size.

In order to apply the proposed technique SCVs are computed from the original images  $\mathbf{X}_1$  and  $\mathbf{X}_2$ , and the threshold value  $T$  in the magnitude domain that separates the  $C_n$  from the  $A_c$  is estimated.  $T$  can be retrieved either by a manual *trial-and-error* procedure or by one of the automatic thresholding algorithms proposed in the literature [7],[10]. Then in the first step  $A_c$  is divided into  $Q$  quantization cells  $q_r$  ( $r=1, \dots, R$ ) of fixed-size  $\Delta\rho \times \Delta\vartheta$ , i.e.,  $A_c = \bigcup_{r=1}^Q q_r$  (see Fig. 5). It is worth noting that the cell size impacts significantly on the method performance. This problem is overcome introducing an adaptive strategy for the estimation of the cell size (see the last step of the estimation procedure).

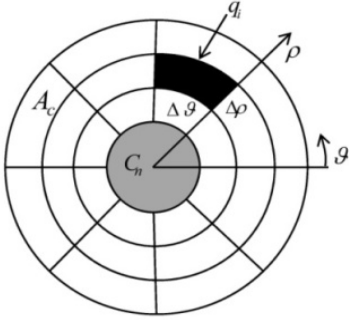


Fig. 5. Quantized magnitude-direction polar domain.

The second step aims at computing a multiscale representation of the information present in the considered images. To this purpose, the two multitemporal images are decomposed according to a multiscale transformation obtaining two sets of images  $\mathcal{X}_{MS_i} = \{ \mathbf{X}_i^0, \dots, \mathbf{X}_i^n, \dots, \mathbf{X}_i^{N-1} \}$ , where the subscript  $i$  ( $i=1,2$ ) denotes the acquisition date, and the superscript  $n$  ( $n=0,1, \dots, N-1$ ) indicates the resolution level ( $\mathbf{X}_i^0 = \mathbf{X}_i$ ). The multiscale decomposition can be carried out by using different algorithms, like gaussian pyramid decomposition, wavelet transform, recursively upsampled bicubic filter, *etc.* Images in  $\mathcal{X}_{MS_i}$  show different tradeoffs between registration noise and geometrical detail content. The maximum level of decomposition has to be selected according to the size of expected changes in the considered dataset.

In the third phase, the CVA technique is applied to each corresponding pair  $(\mathbf{X}_1^n, \mathbf{X}_2^n)$ ,  $n=0, \dots, N-1$ , of low resolution images in  $\mathcal{X}_{MS_1}$  and  $\mathcal{X}_{MS_2}$ . Then the distribution of SCVs within each cell  $q_r$  ( $r=1, \dots, Q$ ) is studied at different scales. For each set of SCVs falling in a given cell  $q_r$  at the highest resolution level, the behavior of the distribution of the same SCVs at the lowest considered resolution level is analyzed in order to identify if the cell is associated with  $RN$  or not. The main idea of this procedure is to identify cells of  $RN$  through a

comparison between the distribution of SCVs at full resolution and at lowest resolution, where pixels of  $RN$  tend to disappear. To this purpose, according to the multiscale properties described in the previous section, the behavior of the mean value of SCVs on the magnitude variable at different resolutions is analyzed. The mean value of SCVs that fall within a cell  $q_r$  at high resolution  $\mu_{\rho, q_r}^0$  is compared with the mean value that the same SCVs have at the lowest resolution level  $\mu_{\rho, q_r}^{N-1}$ <sup>2</sup>. A cell is associated with registration noise ( $RN$ ) or not ( $RNfree$ ) according to the following decision rule:

$$q_r(\Delta\rho, \Delta\vartheta) \in \begin{cases} RN & \text{if } \left| \mu_{\rho, q_r}^0 - \mu_{\rho, q_r}^{N-1} \right| \geq K \\ RNfree & \text{if } \left| \mu_{\rho, q_r}^0 - \mu_{\rho, q_r}^{N-1} \right| < K \end{cases} \quad (7)$$

where  $K$  is a threshold value empirically set to the difference between the mean value of the SCVs that fall in  $A_c$  at the highest resolution and the mean value of the corresponding SCVs at the lowest level, i.e.:

$$K = \left| \mu_{\rho, A_c}^0 - \mu_{\rho, A_c}^{N-1} \right| \quad (8)$$

Let  $q_u^{RN}$  ( $u=1, \dots, U$ ) be a generic cell  $q_r$  ( $r=1, \dots, R$ ),  $U \leq R$ , associated with  $RN$  according to (7). Thus, a generic SCV  $s(i, j)$  in spatial position  $(i, j)$  is associated with registration noise according to:

$$s(i, j) \in \begin{cases} RN & \text{if } s(i, j) \in q_u^{RN}, u = 1, \dots, U \\ RNfree & \text{otherwise} \end{cases} \quad (9)$$

As already mentioned, an important aspect to be considered is the choice of the cell size. Although similar results can be obtained with different quantization values in consistent ranges of  $\Delta\rho, \Delta\vartheta$ , we propose a strategy capable to adaptively identify the cell size, making the technique almost independent from the choice of this parameter. To this purpose, in the last phase of the proposed algorithm, steps from a) to c) are applied for different combination of  $\Delta\rho, \Delta\vartheta$ . The final decision on SCVs is defined according to a majority voting rule. Let us assume that  $A_c$  is divided  $C$  times into quantization cells  $q_{r,c}$  of different size  $\Delta\rho_c \times \Delta\vartheta_c$ , ( $c=1, \dots, C$ ). For each cell size quantization cells are classified according to (7). Thus we obtain  $C$  different classifications where for each spatial position  $(i, j)$  two possible labels are admitted  $RN$  or  $RNfree$  (9). Let us represent labels  $RN$  and  $RNfree$  with +1 and -1, respectively; in order to obtain a single label for each SCV, we consider for each SCV the  $C$  labels  $l(i, j)_c$  and we apply the following majority voting rule:

$$s(i, j) \in \begin{cases} RN & \text{if } \sum_{c=1}^C l(i, j)_c > 0 \\ RNfree & \text{if } \sum_{c=1}^C l(i, j)_c \leq 0 \end{cases} \quad (10)$$

The described procedure, actually results in the definition of cells with variable size and shape in the polar domain as each

<sup>2</sup> It is worth noting that in order to identify cells of  $RN$  we don't analyze the behavior of SCVs that fall within the same cells at different resolution levels, but we consider SCVs that at the highest resolution fall within a cell and the same SCVs at the lowest level. This approach allows us to follow the low-pass effect of the decomposition filter, which causes a migration of SCVs toward the origin of the polar domain.

set of contiguous SCVs in the polar domain at full resolution with the same label defines a cell.

### B. Decision strategy for the generation of the final change-detection map

The information retrieved in the polar domain on each cell about presence/absence of  $RN$  is used for properly driving the generation of the final CD map in the spatial domain of the original images according to a parcel-based procedure. Parcels are defined as regions that adaptively characterize the local neighborhood of each analyzed pixel and are spatially homogeneous in both multitemporal images [20],[21]. The adaptive nature of multitemporal parcels allows us to model complex objects as well as borders of the changed areas and details in the investigated scene. In order to generate multitemporal parcels from the two original images, two segmentation maps are produced by applying a segmentation algorithm separately to  $\mathbf{X}_1$  and  $\mathbf{X}_2$ , independently. Multitemporal parcels are then obtained by imposing homogeneity in the temporal domain according to a fusion of segmentation maps.

The proposed technique exploits the information retrieved from the multiscale analysis in the quantized polar domain in order to establish if a generic parcel belongs to the class of change or not. In greater detail, a generic parcel  $R_p$  is classified according to the following decision rule:

$$R_p \in \begin{cases} \omega_n & \text{if } \frac{N_{R_p}^{RN} + N_{R_p}^{\omega_n}}{N_{R_p}} \geq 0.5 \\ \omega_c & \text{otherwise} \end{cases} \quad (11)$$

where  $N_{R_p}^{\omega_n}$  and  $N_{R_p}^{RN}$  are the number of pixels in the  $p$ th parcel classified as no-changed or as being affected by registration noise, respectively; and  $N_{R_p}$  is the total number of pixels in the  $p$ th parcel. In other words, a parcel  $R_p$  is labeled as no change if the most of the pixels in it either are associated to SCVs affected by registration noise according to (10) or that fall into  $C_n$ .

It is worth stressing that the final change-detection map is computed at full resolution. Low resolution components are used in the analysis only for detecting quantization cells and SCVs associated with  $RN$ . In this way the CD map adequately models the details present in the analyzed VHR images, reproducing accurately both border and homogeneous changed regions.

## IV. EXPERIMENTAL RESULTS

In this section the experimental analysis conducted on real data is presented. First of all the data set is described, then the multiscale properties described in sec. II.B are analyzed. Finally the proposed multiscale and parcel-based technique is applied to the images and the results are presented.

### A. Data set description

In order to assess the effectiveness of the proposed technique, a multitemporal data set composed of two images acquired on the city of Trento (Italy) by the Quickbird

multispectral sensor in October 2005 and July 2006 was considered. The two images were: i) pan-sharpened (Gram-Schmidt procedure implemented in the ENVI software package [23] was applied to the panchromatic channel and the four multispectral bands); ii) radiometrically corrected; and iii) co-registered. In particular, we considered pan-sharpened images as we expect that the pan-sharpening process improves change-detection results [22]. Concerning radiometric corrections we simply normalized the images by subtracting from each spectral channel of the two considered images its mean value. The registration process was carried out by using a polynomial function of order 2 according to 14 ground control points (GCPs), and by applying a nearest neighbor interpolation [23]. In our experiments we did not use more advanced registration techniques and procedures for geometric corrections for better assessing the robustness of the proposed method to residual  $RN$ . The final data set was made up of two pan-sharpened multitemporal and multispectral images of 984x984 pixels (a section of the full scene) with a spatial resolution of 0.7[m], showing a residual misregistration of about 1 pixel on GCPs. Fig. 6.a and b show a true color composition of pansharpened images  $\mathbf{X}_1$  and  $\mathbf{X}_2$ , respectively. Between the two acquisitions two kinds of changes occurred: i) simulated changes i.e., new houses introduced on the rural area (continuous circles in Fig. 6 (b)); ii) real changes i.e., some roofs rebuilt in the urban area (dashed circles in Fig. 6 (b)). Simulated changes have been accurately introduced in order to be as similar as possible to real changes. In particular, some buildings have been added to the scene taking their geometrical structures and spectral signatures from other real buildings present in portions of the available full scene (different from the one considered). This choice allowed us to take into account the image dynamic and the noise properties.

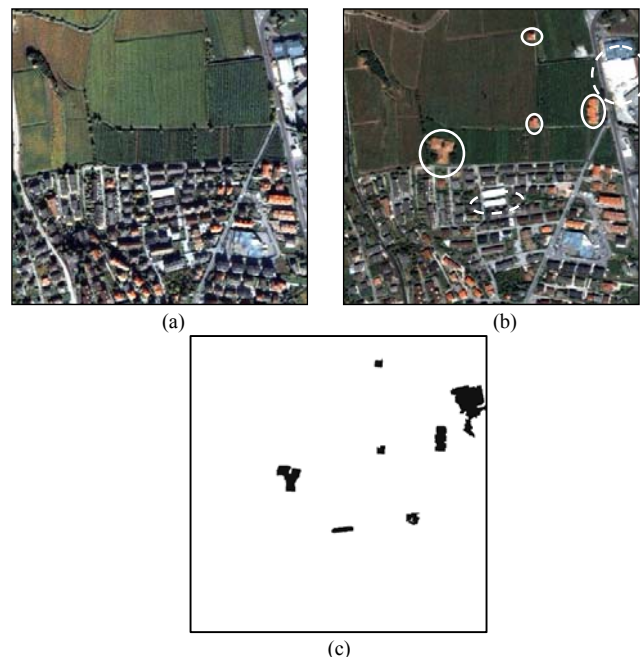


Fig. 6. True color composition of pansharpened images of the Trento city (Italy) acquired by the Quickbird VHR multispectral sensor in: (a) October 2005; and (b) July 2006.

Moreover, it is possible to note that between the two dates also significant seasonal differences in the crop rows and in shadows are present, due to the different acquisition seasons (i.e., summer and autumn). All significant spectral changes occurred between the two images are properly identified by the proposed technique; indeed in the final CD map also seasonal significant radiometric variations will be reported as changes.

In order to allow one a quantitative evaluation of the effectiveness of the proposed method, a reference map (which includes 20602 changed pixels and 968256 unchanged pixels) was defined according to both the available prior knowledge on the considered area and a visual analysis of images (Fig. 6 (c)). In our experiments only the red and near infrared spectral channels were considered, as they demonstrated to be the most effective in emphasizing the changes occurred on the considered dataset.

### B. Results: multiscale properties

In order to show the validity of the fundamentals of the proposed technique, an analysis of the multiscale properties of  $RN$  was conducted in order to show the validity of properties derived on simulated data. To this purpose new data sets with lower resolutions than the original one were generated by applying the *Daubechies-4* stationary wavelet transform to the Quickbird multitemporal images [17]. CVA was applied to the original images and to the dataset at lowest resolution (i.e., the 4<sup>th</sup> level of the stationary wavelet decomposition). Comparing the scattergrams obtained for the two mentioned datasets (see Fig. 7) (and for the other ones obtained at different resolution levels, not reported for space constraints) it is possible to confirm the behavior observed for the simulated dataset (see sec. II.B). As the resolution decreases some clusters (continuous circles in Fig. 7) only reduce their spread, without being completely smoothed out, while other clusters tend to disappear, collapsing into  $C_n$  (dashed circles in Fig. 7.a). From an empirical analysis it is possible to show that SCVs falling into the regions marked with continuous circles in  $A_c$  are SCVs associated to real changes on the ground, while the others are mainly related to  $RN$ . According to this analysis, SCVs of real changes show a quite stable trend, while SCVs associated with  $RN$  have non-stable properties w.r.t. the scale.

The results of this analysis are confirmed also from the behavior of the mean values of the magnitude of SCVs related

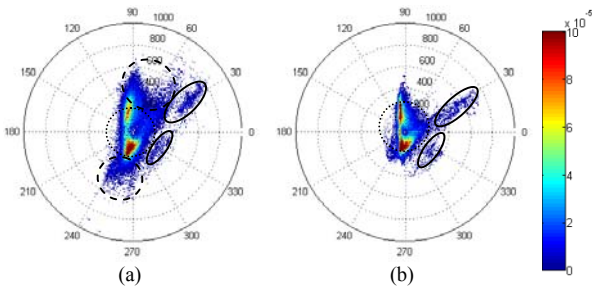


Fig. 7. Scattergrams in polar coordinates of (a) the full resolution original difference image, and (b) the low resolution image obtained at level 4 of the DWT. Dashed circles separate  $C_n$  from  $A_c$ , while continuous circles indicate sectors of true changes.

to  $RN$  and to real changes for decreasing resolution. As expected the former one rapidly decreases by reducing the resolution, while the latter varies slower (Fig. 8).

### C. Results: Change-detection

In order to evaluate the effectiveness of the proposed technique, the methodology presented in sec. III was applied to the real dataset. First of all the CVA technique was applied to pan-sharpened images  $\mathbf{X}_1$  and  $\mathbf{X}_2$ . According to the proposed technique, the decision threshold  $T$  that separates  $A_c$  from  $C_n$  was computed applying the Bayes rule for minimum error [7],[10], retrieving a value  $T$  equal to 220. This value is reasonable as according to the ground truth available information we verified that SCVs related to true changes have magnitude higher (although sometime very close) than  $T$ . Then  $A_c$  was divided into quantization cells of size  $\Delta\rho \times \Delta\theta$ . According to the proposed technique different quantization values have been considered in order to adaptively identify a proper cell size. In our experiments combinations with  $\Delta\rho = \{100, 200, 300, 400, 500\}$  and  $\Delta\theta = 10^\circ$  were tested. However several different combinations of cell size gave similar results as for a quite large range both in the magnitude and direction domain the behavior of SCVs is stable (see Tab. 1). For each cell the difference in the mean value of the magnitude of SCVs between the resolution level 0 and 4 was computed. These values were compared with the threshold  $K$  derived according to (8) (for  $T$  equal to 220,  $K$  resulted equal to 190). SCVs falling into cells in which the difference was greater than  $K$  were classified as belonging to  $RN$  according to (9) and (10).

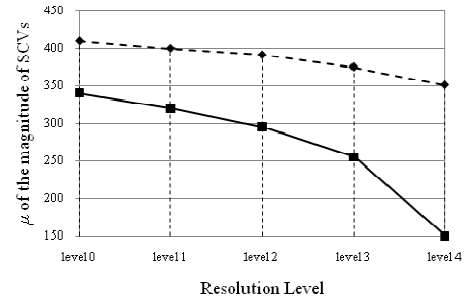


Fig. 8. Behavior of the mean value of the magnitude of SCVs versus the resolution levels (scale) for the class of changes (dashed line) and of registration noise (continuous line).

The identified cells were used in the parcel-based decision strategy for computing the change-detection map. At first multitemporal parcels were generated by applying a multiscale region growing segmentation technique to  $\mathbf{X}_1$  and  $\mathbf{X}_2$  separately [24], and fusing the results as described in [21]. Then SCVs of each parcel were analyzed applying (11). Tab. 1 summarizes results obtained at a pixel level by applying the proposed technique to the five different single quantization values, without the adaptive estimation of the cell size. As one can see, different quantizations in a consistent range of  $\Delta\rho_c \times \Delta\theta_c$  (i.e., between  $200 \times 10^\circ$  and  $400 \times 10^\circ$ ) gave similar results; however, to overcome possible bias introduced by a

particular setup, it is useful to adaptively model the cell size. To this purpose, we applied the proposed technique by considering the majority rule in (10) (see Tab. 2). The obtained results were compared with the ones yielded ignoring the presence of registration noise. To this purpose, we considered the standard CVA that assigns SCVs that fall into  $C_n$  to  $\omega_n$  and all SCVs in  $A_c$  to the class of changes. Both the results at pixel [10] and at parcel level [20] (see Tab. 2) demonstrate that the standard method is sharply affected by the presence of registration noise, which results in a high number of false alarms mainly located on the high frequency regions of images. On the contrary, the proposed method significantly reduces false alarms both at pixel (from 173676 to 61429) and at parcel level (from 106580 to 28150) and generates a map characterized by high accuracy both in homogeneous and border areas (see Fig. 10). As expected, the contextual analysis allows one to obtain a regularized CD map without affecting the details in the image thanks to the adaptive nature of parcels.

For a further confirmation of the validity of the proposed technique, we compared the obtained results with the one achieved with a manual procedure. A pixel-based CD maps was generated by assigning SCVs that fall into  $C_n$  to  $\omega_n$  and all statistically significant clusters present both at full and at the lowest considered resolution level in  $A_c$  to the class of changes. To this purpose, manual thresholds in the polar domain were applied at full resolution both in the magnitude and direction domain. A similar approach was adopted for building a parcel-based CD map. Results yielded by the manual approach can be considered as an upper bound. From Tab. 2 one can conclude that the proposed method performs effectively, as the obtained overall accuracies are close to this upper bound both at a pixel (93.13% vs. 93.62%) and at a parcel level (96.69% vs. 97.18%).

Tab. 1. Change detection results obtained at a pixel level with the proposed multiscale technique without the adaptive analysis of the cell size.

Cell size ( $\Delta\rho \times \Delta\theta$ )	False alarms	Missed alarms	Overall error	Overall accuracy (%)
100x10	111279	17356	128635	86.72
200x10	61252	5123	66375	93.15
300x10	62867	4728	67595	93.02
400x10	63091	4644	67735	93.00
500x10	76614	17905	94519	90.24

Tab. 2. Change detection results obtained with the proposed adaptive and multiscale technique, the standard CVA, and the manual approach at both pixel and parcel level.

Technique		False alarms	Missed alarms	Overall error	Overall accuracy (%)
Pixel-based	Proposed	61429	5061	66490	93.13
	Standard CVA	173676	1470	175146	81.91
	Manual	55984	5768	61752	93.62
Parcel-based	Proposed	28150	3870	32020	96.69
	Standard CVA	106580	734	107314	88.92
	Manual	23160	4192	27352	97.18

It is worth noting that, although changed objects are identified with high fidelity and false alarms are considerably reduced, some false alarms remain in the CD map derived with the proposed approach. They are mainly due to the different acquisition seasons (i.e., summer and autumn) of the considered images, which resulted in significant radiometric differences related to seasonal variations in the crop rows and in shadows.

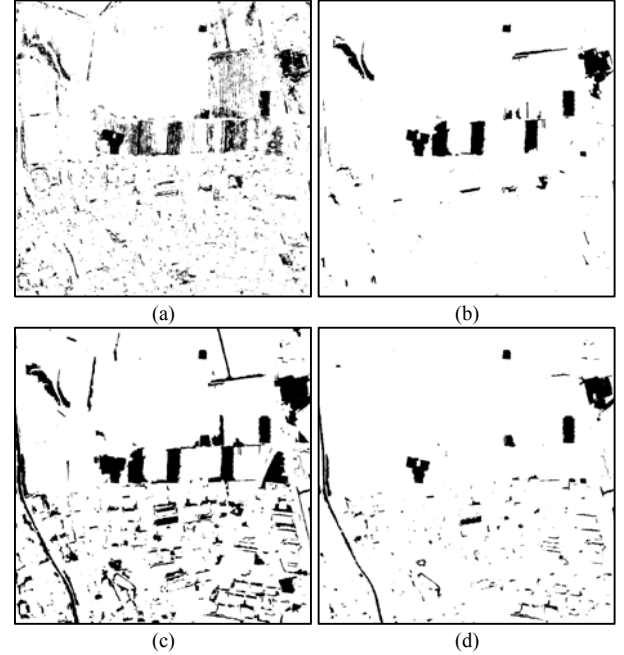


Fig. 9. Change-detection maps obtained with: (a) proposed approach with the adaptive estimation of the cell size (pixel level); (b) proposed parcel-based technique with the adaptive analysis of the cell size; (c) parcel-based CVA; and (d) manual approach at a parcel level.

## V. CONCLUSION

In this paper we presented a context-sensitive multiscale technique robust to registration noise for change detection on very high geometrical resolution images (it is worth noting that the proposed method can be suitable also for the analysis of optical medium resolution data). The entire procedure has taken advantages from a previous study on the effects of registration noise in multitemporal VHR image and was carried out in the context of a polar framework for change vector analysis (CVA). On the basis of the multiscale properties of  $RN$ , in this paper we defined a technique based on a multiscale analysis of SCVs distribution in a quantized polar domain able to limit the effect of registration noise in the generation of the final change-detection map. From this analysis it is possible to extract information on registration noise, which is considered in the algorithm for the generation of the change-detection map. In order to make the process independent from the size of quantization cells, we developed a strategy that automatically considers different cell sizes and results in adaptive cells with variable size and shape. In order to increase the accuracy of the change-detection process, the proposed technique also exploits the contextual information

present in VHR images according to multitemporal parcels and integrates this information in the generation of the final change-detection map. In order to assess the reliability of the proposed method several experiments were conducted on a pair of multitemporal Quickbird images. Both qualitative and quantitative analysis carried out on a real multitemporal data set of VHR images confirm the effectiveness of the proposed technique. In greater details, the quantitative analysis shows that the proposed method consistently reduces the false alarm rate with respect to standard methods that neglects registration noise information. The qualitative analysis confirms these observations and points out the ability of the parcel-based strategy in modeling adequately both homogeneous and border regions.

As a future work we plan to test the proposed method on multitemporal images acquired by different sensors representing different change detection problems.

#### REFERENCES

- [1] L. H. Chen and S. Chang, "A video tracking system with adaptive predictors," *Pattern Recognition*, vol. 25, no. 10, pp. 1171-1180, 1992.
- [2] S. C. Liu, C. W. Fu, and S. Chang, "Statistical change detection with moments under time-varying illumination," *IEEE Trans. on Image Processing*, vol. 7, no. 9, pp. 1258-1268, 1998.
- [3] C. Dumontier, F. Luthon, and J.-P. Charras, "Real-Time DSP Implementation for MRF-Based Video Motion Detection," *IEEE Trans. on Image Processing*, vol. 8, no. 10, pp. 1341-1347, 1999.
- [4] L. Bruzzone and S. B. Serpico, "An iterative technique for the detection of land-cover transitions in multitemporal remote-sensing images," *IEEE Trans. on Geosci. Rem. Sens.*, vol. 35, no. 4, pp. 858-867, 1997.
- [5] L. Bruzzone and S. B. Serpico, "Detection of changes in remotely sensed images by the selective use of multi-spectral information," *Int. J. of Rem. Sens.*, vol. 18, no. 18, pp. 3883-3888, 1997.
- [6] M. Bosc, F. Heitz, J. P. Armspach, I. Namer, D. Gounot, and L. Rumbach, "Automatic change detection in multimodal serial MRI: Application to multiple sclerosis lesion evolution," *Neuroimage*, vol. 20, pp. 643-656, 2003.
- [7] R.J. Radke, S. Andra, O. Al-Kofahi and B. Roysam, "Image Change Detection Algorithms: A Systematic Survey," *IEEE Trans. on Image Processing*, vol. 14, no. 3, pp. 294-307, 2005.
- [8] P.R. Coppin, I. Jonckheere and K. Nachaerts, "Digital change detection in ecosystem monitoring: A review," *Int. J. Rem. Sens.*, vol. 25, no. 9, pp. 1565-1596, 2004.
- [9] D. Lu, P. Mausel, E. Brondizio and E. Moran, "Change detection techniques," *Int. J. Rem. Sens.*, vol. 25, no. 12, pp. 2365-2407, 2004.
- [10] L. Bruzzone, D.F. Prieto, "Automatic Analysis of the Difference Image for Unsupervised Change Detection," *IEEE Trans. Geosci. Rem. Sens.*, vol. 38, pp.1171-1182, 2000.
- [11] J.R.G. Townshend, C.O. Justice, and C.Gurney, "The impact of misregistration on change detection," *IEEE Trans. Geosci. Rem. Sens.*, vol. 30, pp. 1054-1060, 1992.
- [12] X. Dai, S. Khorram, "The effects of image misregistration on the accuracy of remotely sensed change detection," *IEEE Trans. Geosci. Rem. Sens.*, vol. 36, pp. 1566-1577, 1998.
- [13] L. Bruzzone, R. Cossu, "An adaptive approach for reducing registration noise effects in unsupervised change detection," *IEEE Trans. Geosci. Rem. Sens.*, vol. 41, no. 11, pp.2455-2465, 2003.
- [14] J. Li, S. Qian, X. Chen, "Object-oriented method of land cover change detection approach using high spatial resolution remote sensing data," *IEEE Trans. Geosci. Rem. Sens.*, vol. 5, pp. 3005-3007, 2003.
- [15] F. Bovolo, L. Bruzzone, "A multilevel parcel-based approach to change detection in very high resolution multitemporal images," *IEEE Int. Geosci. Rem.Sens. Symp.*, vol. 3, pp. 2145-2148, 2005.
- [16] I. Niemeyer, P.R. Marpu, S. Nussbaum, "Change detection using the object features," *IEEE Int. Geosci. Rem. Sens. Symp.*, pp. 2374-2377, 2007.
- [17] F. Bovolo and L. Bruzzone, "A theoretical framework for unsupervised change detection based on change vector analysis in polar domain," *IEEE Transactions on Geoscience and Remote Sensing*, vol. 45, no. 1, pp. 218-236, 2007.
- [18] F. Bovolo, L. Bruzzone and S. Marchesi, "Analysis and adaptive estimation of the registration noise distribution in multitemporal VHR images," *IEEE Trans. Geosci. Rem. Sens.*, in press.
- [19] S.G. Mallat, "A theory for multiresolution signal decomposition: the wavelet representation," *IEEE Trans. Pattern Anal. Machine Intell.*, vol. PAMI-11, no. 7, pp. 674-693, 1989.
- [20] L. Bruzzone and D. F. Prieto, "An adaptive parcel-based technique for unsupervised change detection," *Int. J. Rem. Sens.*, vol. 21, no. 4, pp. 817-822, 2000.
- [21] F. Bovolo and L. Bruzzone, "A multilevel parcel-based approach to change detection in very high resolution multitemporal images," *IEEE Int. Geosci. Rem. Sens. Symp.*, vol. 3, July 2005, pp. 2145-2148.
- [22] F. Bovolo, L. Bruzzone, L. Capobianco, A. Garzelli, S. Marchesi and F. Nencini, "Change detection from pansharpened images: a comparative analysis", *ESA-EUSC 2008: Image Information Mining*, Mar. 4-6 2008.
- [23] ENVI User Manual. Boulder, CO: RSI, 2003. [Online.] Available: <http://www.RSInc.com/envi>.
- [24] Baatz, M., U. Benz, S. Dehghani, M. Heynen, A. Höltje, P. Hofmann, I.Lingenfelder, M. Mimler, M. Sohlbach, M. Weber, and G Willhauck (2004). *eCognition User Guide 4. Definiens Imaging*.